Advances in Concrete Construction, *Vol. 20, No. 2 (2025) 65-78*
https://doi.org/10.12989/acc.2025.20.2.065

Study on dynamic mechanical properties and damage evolution model of C80 concrete

Haipeng Jia*, Tong Shen**, Yuxia Zhao, Fei Liu, Wenlong Wu and Qianqian Song

Department of Urban and Underground Space, School of Civil and Transportation Engineering, Henan University of Urban Construction, Pingdingshan 467000, China

(*Received February 23, 2025, Revised May 6, 2025, Accepted June 17, 2025*)

Abstract. In order to accurately assess the response of a structure when subjected to impact or vibration loading, there is an urgent need to carry out studies on the dynamic mechanical properties of high-strength concrete. Impact tests on C80 concrete with different combinations of stress wavelengths and strain rates were conducted using a 75 mm SHPB test system and compared with dynamic impact tests on C35 plain concrete. The following conclusions can be obtained: Under the action of multiple impacts, the cumulative damage of C80 concrete and the number of impacts show the form of "rapid rise - smooth development-rapid rise." The dynamic strength of C80 concrete is positively correlated with the peak strain and strain rate, and the increase of stress wavelength and impact velocity raises the overall development trend of peak strain. As the impact velocity increases, the cumulative damage increases significantly while the number of repeated impacts gradually decreases. The established C80 concrete cumulative damage evolution model can calculate the physical significance of the model parameters and simultaneously reflect the impact velocity and impact number. Additionally, it confirms the model's logic and accuracy of the physical parameters, which might serve as a particular benchmark for related studies. Comparative analysis shows C35 exhibits greater deformability than C80 at equivalent strain rates (80 s^{-1}). The growth in peak strain for C35 surpasses that of C80 as strain rates escalate from 50 s^{-1} to 80 s^{-1}, with C35's strain-rate curve showing a steeper slope. Microstructural analysis attributes C80's restrained deformation to its denser matrix, which enhances strength retention but limits crack propagation. These findings provide critical insights for material selection in protective structures.

Keywords: C80 concrete; damage model; SHPB; strain rate effect; stress wave effect

1. Introduction

The stability and safety of buildings and structures are directly impacted by the mechanical characteristics of concrete materials. The study of the dynamic mechanical properties of high-strength concrete has become more and more relevant and urgent in light of the current complex world scenario and military conflicts. Fewer member ends and reduced costs are benefits of high-strength concrete, which also has the qualities of great strength, slight deformation, and long durability. As a result, it is anticipated that high-strength concrete materials would become more prevalent in concrete technology (Tahwia *et al*. 2022). The mechanical characteristics of high-strength concrete under static loads have been studied further (Rabia *et al*. 2021). Parida and Jena (2023) have conducted research on high performance concrete materials from the aspect of materials, and have obtained fruitful research results . However, research into their mechanical properties under dynamic pressures has been scant. The concrete is a strain-rate-sensitive material, which means that its mechanical properties under high strain rates differ from those under static loads (Antoniou *et al*. 2025). Zhou *et al*. (2024) believed that when subjected to dynamic compressive loading, concrete specimens with varying aggregate and mortar ratios exhibited diverse alterations in stress states. Caverzan *et al*. (2016) discovered that large-size specimens struggled to attain a uniform state of stress-strain throughout the majority of the loading process, resulting in a deviation from actual conditions in the obtained stress-strain curve, this was evidenced by the diffusion phenomenon observed during the propagation of stress waves in the large-diameter Split Hopkinson Pressure Bar apparatus. Martin *et al*. (2018) characterized three high-performance concrete (HPC) materials with different specimen geometries using Kolsky compression bar techniques to investigate the strain rate and specimen size effects on their uniaxial compressive strength. Du *et al*. (2022) conducted Split Hopkinson Pressure Bar (SHPB) tests on concrete specimens at different strain rates, revealing that the compressive strength, flexural strength, and dynamic modulus of elasticity of concrete specimens increased with an increase in loading frequency. Mohammad *et al*. (2024) conducted impact tests on concrete materials at high strain rates using Split Hopkinson Pressure Bar and demonstrated that the breaking stress and breaking strain of concrete materials exhibited an increasing trend with the increase in strain rate. Chen *et al*. (2022)

*Corresponding author, Ph.D., Professor,
E-mail: 20221043@huuc.edu.cn

**Co-corresponding author, Ph.D., Professor,
E-mail: 20201001@huuc.edu.cn

ISSN: 2287-5301 (Print), 2287-531X (Online)

investigated the dynamic mechanical properties of high-strength concrete at various strain rates using Split Hopkinson Pressure Bar test system, and analyzed the variations in dynamic compressive strength, peak strain, elastic modulus, and damage pattern.

Damage theory and damage model development were pioneered by Kachanov (1999) and Rabotnov (1969), which have since been extensively researched by academics. To gain a deeper understanding of the correlation between damage evolution and strain rate, Wang and Hu (2003) conducted concrete damage experiments using large-scale Split Hopkinson Pressure Bar and subsequently derived an equation to describe the material's damage evolution. Zhang *et al*. (2020) investigated the elastic-plastic damage behavior of concrete-like materials using the elastic-plastic fully implicit iterative method. Cao *et al*. (2020) utilized a generalized regression neural network to predict damage in restrained concrete materials and subsequently developed a damage model. Sharma *et al*. (2021) evaluated the potential of three machine learning techniques and found the best algorithm for the prediction of flexural strength of concrete mix with steel fibre. Lata (2021) dealed with the study of Stoneley wave propagation at the interface of two dissimilar homogeneous orthotropic thermoelastic solids. By using appropriate boundary conditions the secular equations of Stoneley waves are derived in the form of the determinant. Samuel *et al*. (2022) used the computation systems MAPLE and ANSYS to study the failure of laminated composite material plates. Huang *et al*. (2023) analyzed the stress wave transmission and reflection effect on the modified Split Hopkinson Pressure Bar system to obtain the macroscopic damage morphology, particle size distribution law of crushing products, and energy dissipation law of concrete specimens containing different admixtures.

The widespread adoption of high-strength concrete in critical infrastructures (skyscrapers, blast-resistant facades, nuclear containment) necessitates urgent research into its dynamic behavior under extreme loads (earthquakes, explosions, impacts). Unlike conventional concrete, high-strength concrete exhibits pronounced brittleness and distinct strain-rate effects, potentially leading to catastrophic failure modes. While prior studies predominantly focus on concrete's static properties, its dynamic response — particularly damage sensitivity — remains underexplored. This study bridges this gap by quantitatively characterizing high-strength concrete's damage evolution under impact loading, offering critical insights for protective structure design.

Fig. 1 C80 concrete cylindrical specimen

2. Research on the dynamic mechanical properties of C80 concrete

2.1 C80 concrete SHPB test set

The SHPB dynamic impact test needs a flat specimen end face, an adequate length-to-diameter ratio, one-dimensional stress wave assumptions, and uniformity assumptions. The specimen utilized in the test has a diameter of 50 mm and a length of 75 mm. and the unevenness of the end face was within 0.02 mm. Vaseline was applied to the specimen's end face on the 3 m-long input and output rods to decrease the influence of end friction. The bulk specimens of C80 concrete were made by coring, cutting, and grinding. Specimens with sound velocity variations within 5% were chosen after ultrasonic testing to verify the consistency of the test (Fig. 1). The fundamental physical and mechanical indices of cylindrical C80 concrete specimens can be accurately measured and reliably estimated to yield the following standard values: the longitudinal wave speed is 3851 m/s, the elastic modulus is 38.1 GPa, the uniaxial compressive strength is 49.7 MPa, and the Poisson's ratio is 0.23.

Concrete is a non-homogeneous medium, so to satisfy the hypothesis of homogeneity, a large-diameter SHPB experimental setup with a diameter of 75 mm and a specimen length-to-diameter ratio of 0.67 is used. The stress wave in the specimen can quickly approach stress homogeneity by matching the wave impedance of the specimen, incident rod, and transmission rod. The standard wave impedance of the C80 concrete used in this experiment was 9.45 $MPa \cdot m^{-1} \cdot s^{-1}$, and the CrMn steel rod test equipment was chosen after comparison. The wave impedance of a CrMn steel rod is 39.5 $MPa \cdot m^{-1} \cdot s^{-1}$, and its ratio to the specimen is 0.24. According to Ping *et al*. (2013), a calculation that demonstrates the stress wave can pass through the specimen six times in succession, it takes specimen 78 to reach stress homogeneity. The SHPB test system is shown in Fig. 2.

2.2 Wave propagation and data processing in SHPB experiments

Upon impact by the impact bar, an incident compressive wave is generated within the incident bar, propagating rightward along the bar axis. As illustrated in Fig. 3, this wave undergoes partial reflection and transmission at the interfaces between the bars and specimen (denoted as interfaces 1-1 and 2-2, respectively).

Under the one-dimensional stress wave theory assumption, the displacements at interfaces 1-1 (U_1) and 2-2 (U_2) can be expressed as

$$U_1 = c_0 \int_0^t (\varepsilon_i - \varepsilon_r) d\tau \tag{1}$$

$$U_2 = c_0 \int_0^t (\varepsilon_t) d\tau \tag{2}$$

Where c_0 is the longitudinal elastic wave speed of the bar material, and ε_i, ε_r and ε_t represent the incident,

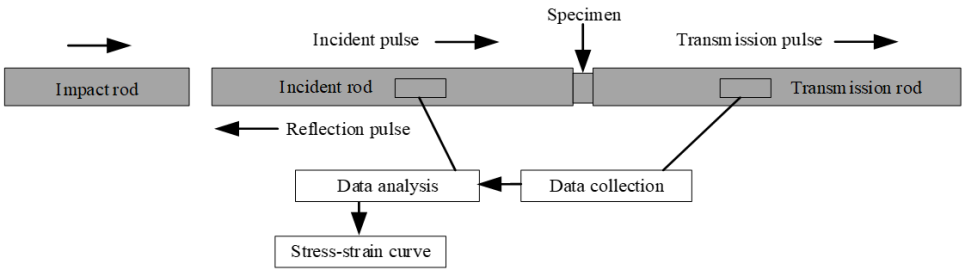

(a) Schematic diagram of SHPB system

(b) Physical diagram of the SHPB system

Fig. 2 The diagram of the SHPB experimental system

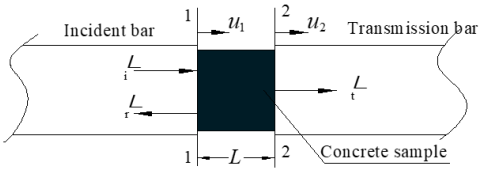

Fig. 3 Theory of SHPB Experiment

reflected, and transmitted strain pulses, respectively.

For a specimen with cross-sectional area A0 and length l0, the average strain $\varepsilon(t)$ is derived as:

$$\varepsilon(t) = \frac{U_1 - U_2}{l_0} = \frac{c_0}{l_0}\int_0^t (\varepsilon_i - \varepsilon_r - \varepsilon_t)\, d\tau \tag{3}$$

The strain rate $\dot{\varepsilon}$ is obtained by differentiating Eq. (3) with respect to time

$$\dot{\varepsilon} = \frac{c_0}{l_0}(\varepsilon_i - \varepsilon_r - \varepsilon_t) \tag{4}$$

The forces at both specimen-bar interfaces, F_1 and F_2, are calculated as

$$F_1 = AE(\varepsilon_i + \varepsilon_r) \tag{5}$$

$$F_2 = AE\varepsilon_t \tag{6}$$

where A is the cross-sectional area of the bars and E denotes the elastic modulus of the bar material.

Consequently, the average stress in the specimen is given by

$$\sigma = \frac{1}{2A_0}(F_1 + F_2) = \frac{AE}{2A_0}(\varepsilon_i + \varepsilon_r + \varepsilon_t) \tag{7}$$

By processing the acquired incident, reflected, and transmitted strain signals through Eqs. (3), (4), and (7), the time histories of the specimen's average strain, strain rate, and stress can be determined.

2.3 Experimental design for the study of dynamic mechanical properties of C80 concrete

In the SHPB test, a stress wave is generated after the impact rod strikes the incident rod, with a length twice that of the impact rod. This investigation includes 15 sets of tests covering three stress wavelengths and five impact rod speeds, selected to encompass stress wavelengths provided by the SHPB system and provide distinct differences for each trial group. The dynamic impact velocity range should correspond to the gradual velocity gradient of specimens. The dynamic mechanical properties of the specimen should be investigated under various stress wavelengths and impact velocities, with a focus on covering the velocity gradient range from gradual to complete destruction. The design plan is presented in Table 1.

2.4 Examining the impact of C80 concrete's strain rate

The impact tests were conducted at five different velocities for each stress wavelength, and the resulting data on strain rate, peak strain, and peak stress are presented in the table below. Three-cylinder impact rods with lengths of 800 mm, 1200 mm, and 1600 mm were utilized respectively during testing.

The dynamic strength growth factor (DIF) is defined as Eq. (8) to analyze the strength change law of C80 concrete specimens under the influence of dynamic impact.

$$DIF = \frac{f_d}{f_s} \tag{8}$$

Where fs represents the static compressive strength of the material, f_d represents its dynamic compressive strength.

The relationship between the dynamic strength growth factor and strain rate of C80 concrete under various stress wavelengths can be observed as Fig. 4.

Table 1 Experimental design of C80 concrete dynamic mechanical properties

The stress wavelength (mm)	The impact velocity ($m \cdot s^{-1}$)	The strain rate (s^{-1})	The peak strain	The peak stress (MPa)
λ_1	V_1	$\dot{\varepsilon}_1$	ε_1	σ_1
	V_2	$\dot{\varepsilon}_2$	ε_2	σ_2
	V_3	$\dot{\varepsilon}_3$	ε_3	σ_3
	V_4	$\dot{\varepsilon}_4$	ε_4	σ_4
	V_5	$\dot{\varepsilon}_5$	ε_5	σ_5
λ_2				
λ_3				

The dynamic strength of C80 concrete exhibits sensitivity to strain rate, as illustrated in Fig. 4, which portrays the correlation between the dynamic strength growth factor and strain rate of C80 concrete. As depicted in the Fig. 4, there exists a positive relationship between the dynamic strength growth factor (DIF) and strain rate, which can be expressed by Eq. (9). Furthermore, it is observed that higher impact velocities result in greater strain rates and consequently lead to an increase in the dynamic strength growth factor.

$$DIF = 0.00347\dot{\varepsilon}^{0.8739} \quad (52 < \dot{\varepsilon} < 86) \tag{9}$$

2.5 Analysis of C80 concrete's dynamic impact stress wavelength influence

The deformation and damage state of C80 concrete under impact is highly correlated with the stress wavelength of stress waves. As the stress wavelength increases from

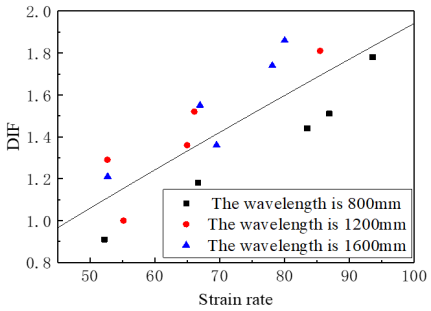

Fig. 4 Relationship between dynamic strength growth factor and strain rate

800 mm to 1600 mm within essentially the same strain rate range, the peak strain corresponding to dynamic strength gradually increases. For a given strain rate level, Fig. 5 illustrates the linear positive correlation between peak strain and stress wavelength within the range of 102 s^{-1}. Eqs. (10)-(12) establish the quantitative relationships between stress wavelength and peak strain for wavelengths of 800 mm, 1200 mm, and 1600 mm, respectively.

With an 800 mm stress wavelength

$$\varepsilon_p = (0.0927\dot{\varepsilon} + 0.9471) \times 10^{-3} \tag{10}$$

With an 1200 mm stress wavelength

$$\varepsilon_p = (0.0851\dot{\varepsilon} + 2.9896) \times 10^{-3} \tag{11}$$

With an 1600 mm stress wavelength

$$\varepsilon_p = (0.0599\dot{\varepsilon} + 6.395) \times 10^{-3} \tag{12}$$

In conclusion, the dynamic mechanical properties of C80 concrete are affected by both strain rate and stress

Table 2 Test results of dynamic mechanical properties of C80 concrete

The stress wavelength (mm)	The number	The impact velocity ($m \cdot s^{-1}$)	The strain rate (s^{-1})	The peak strain (10^{-3})	The peak stress (MPa)	DIF
800	1	4.83	52.19	6.23	45.25	0.91
	2	6.15	66.66	6.55	58.48	1.18
	3	7.91	83.48	7.97	71.81	1.44
	4	8.82	86.88	9.67	74.84	1.51
	5	9.59	93.57	9.81	88.39	1.78
1200	6	4.88	55.13	8.35	49.88	1.00
	7	5.76	52.67	7.10	64.35	1.29
	8	6.49	64.95	7.96	67.68	1.36
	9	7.75	66.06	8.77	75.51	1.52
	10	8.28	85.46	10.35	90.13	1.81
1600	11	5.36	52.70	9.48	60.37	1.21
	12	6.28	69.49	11.28	67.41	1.36
	13	7.08	66.94	10.00	77.23	1.55
	14	8.12	78.09	10.81	86.49	1.74
	15	8.28	80.05	11.19	92.22	1.86

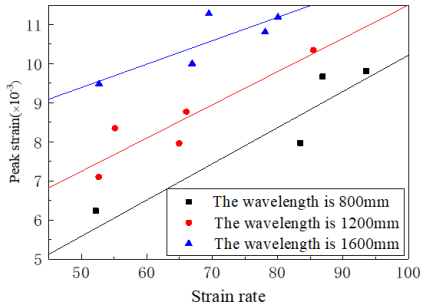

Fig. 5 Relationship between stress wavelength and peak strain

wavelength. Specifically, at medium strain rates, the dynamic strength growth factor of C80 concrete exhibits a positive correlation with strain rate. On the one hand, peak strain in C80 concrete also shows a positive correlation with strain rate. On the other hand, there exists a positive correlation between the peak strain of C80 concrete and the strain rate, and as the stress wavelength increases, so does the peak strain. This phenomenon can be attributed to an increase in energy exposure for C80 concrete specimens with longer stress wavelengths while still being subjected to identical wave amplitudes.

3. Research on the damage characteristics of C80 concrete

3.1 Dynamic damage test design

The dynamic damage analysis of C80 concrete was conducted by designing three impact velocities while considering two stress wavelengths, resulting in a reduction in sound velocity without visible cracks in the specimen. This ensured that the impact velocity was only slightly greater than the damage threshold velocity corresponding to each stress wavelength. The concrete specimen underwent multiple impacts until it reached its breaking point. At each stress wavelength, three parallel tests were conducted to measure the damage value of the material using the RSM-SY5 acoustic wave instrument and a supporting longitudinal wave transducer developed by the Wuhan Institute of Geotechnics, Chinese Academy of Sciences (Fig. 6).

Fig. 6 RSM-SY5 Acoustic Wave Tester

3.2 Determination of the damage variable

The damage variables of the specimens before and after each impact are given by Eq. (13) for the dynamic damage impact research of C80 concrete.

$$D = 1 - \left(\frac{\bar{V}_P}{V_P} \right)^2 \tag{13}$$

Where VP denotes the concrete's longitudinal wave velocity before impact and denotes the concrete's longitudinal wave velocity following impact.

3.3 Law of concrete damage progression

Three parallel tests were conducted for each stress wave, with the specimens subjected to impacts of 800 mm and 1200 mm stress wavelength. To ensure comparable strain rates of materials, it is essential to maintain a constant impact velocity of the impact rod throughout each test. The results of these tests are presented in Table 4.

Air pressure was utilized to regulate the impact velocity of the impact rod during testing, resulting in slight variations in actual impact velocity from test to test. The average impact velocities for three trials conducted under an 800 mm stress wavelength were 3.98 cm/s, 6.11 cm/s, and 7.03 cm/s respectively; while those conducted under a 1200 mm stress wavelength yielded average impact velocities of 4.09 cm/s, 5.04 cm/s, and 6.14 cm/s respectively.

(1) Research on C80 concrete damage caused by the same impact velocity

Table 4 demonstrates that the cumulative damage endured by C80 concrete specimens under repeated

Table 3 C80 concrete dynamic damage test design

The number	The stress wavelength	The number of impacts	The impact velocity	The peak strength	The peak strain	The wave velocity		The damage
						Before the impact	After the impact	
1	λ_1	n1	V_1	/	/	/	/	/
	λ_1	n2	V_2	/	/	/	/	/
	λ_1	n3	V_3	/	/	/	/	/
2	λ_2	n1	V_1	/	/	/	/	/
	λ_2	n2	V_2	/	/	/	/	/
	λ_2	n3	V_3	/	/	/	/	/

impacts with identical stress wave length and impact rod velocity is exclusively reliant on the number of strikes (n). The subsequent chart illustrates the correlation between total damage and the total number of strikes during the initial test, which employed two different stress wavelengths.

The damage evolution of C80 concrete under repeated impact exhibits a pattern of "rapid rise-smooth development-rapid rise," as illustrated in Fig. 7. To facilitate the study of this pattern, the number of repeated impacts is normalized under the influence of two stress wavelengths, as shown in Fig. 8.

The aforementioned graphic shows the connection between the relative impact number in the first test and the cumulative damage of C80 concrete. As can be observed, when the relative impact number acts as the independent variable, all the data still exhibit the same development trend, which takes the form of "rapid rise - smooth

Table 4 Repeated impact test results of C80 high-strength concrete

The number	The stress wavelength	The number of impacts	The impact velocity	The peak strength	The peak strain	The wave velocity		The damage
						Before the impact	After the impact	
1	800	1	4.04	99.03	2.879	3846	3333	0.133385
		2	3.74	95.15	3.239	3333	3125	0.195792
		3	3.82	93.92	3.549	3125	2941	0.254672
		4	3.88	89.70	3.625	2941	2778	0.310095
		5	4.06	79.57	3.670	2778	2632	0.362651
		6	3.73	78.60	3.772	2632	2548	0.394566
		7	3.81	74.62	3.883	2548	2381	0.460107
		8	4.22	72.17	3.904	2381	2174	0.547045
		9	3.92	71.21	3.971	2174	1923	0.662501
		10	4.31	68.62	4.260	1923	1615	0.822667
		11	4.21	61.00	4.405	1615	1515	0.884587
		12	3.97	56.80	4.562	1515	0	1
2	800	1	6.29	96.76	4.161	3846	3333	0.133385
		2	6.19	89.68	4.201	3333	2941	0.250997
		3	6.30	85.08	4.310	2941	2381	0.441409
		4	5.78	77.23	4.385	2381	1927	0.632085
		5	5.87	71.00	4.457	1927	1515	0.845889
		6	6.22	67.22	4.671	1515	1492	0.86107
		7	6.09	56.73	4.711	1492	1321	0.975681
		8	6.13	54.55	4.837	1321	0	1
3	800	1	7.38	95.02	4.405	3846	3125	0.187467
		2	6.89	80.42	4.562	3125	2381	0.425547
		3	7.55	78.98	4.688	2381	1923	0.617904
		4	6.70	69.74	4.781	1923	1515	0.830072
		5	6.65	60.03	4.844	1515	0	1
1	1200	1	4.24	121.78	3.863	4145	3333	0.195899
		2	3.89	104.47	4.301	3333	3125	0.258305
		3	4.02	86.52	4.459	3125	2947	0.315265
		4	4.20	84.36	4.624	2947	2732	0.38822
		5	4.26	83.15	4.875	2732	2581	0.443491
		6	3.72	82.54	5.396	2581	2374	0.523693
		7	4.25	78.19	5.422	2374	1927	0.711983
		8	4.08	74.42	5.477	1927	1623	0.869741
		9	4.17	72.72	5.736	1623	1515	0.936284
		10	4.02	68.34	5.785	1515	0	1

Table 4 Continued

The number	The stress wavelength	The number of impacts	The impact velocity	The peak strength	The peak strain	The wave velocity		The damage
						Before the impact	After the impact	
2	1200	1	5.07	115.7	5.322	3846	3125	0.187467
		2	5.14	98.06	5.420	3125	2941	0.246347
		3	4.99	88.02	5.536	2941	2381	0.436759
		4	4.99	74.54	5.685	2381	1927	0.627435
		5	4.94	69.91	5.755	1927	1515	0.841239
		6	5.09	63.06	5.894	1515	0	1
3	1200	1	6.17	98.19	5.965	3846	2941	0.235309
		2	6.36	85.97	6.002	2941	2500	0.385258
		3	6.27	79.28	6.052	2500	1927	0.614458
		4	5.97	74.36	6.148	1927	1316	0.931532
		5	5.94	65.75	6.158	1316	0	1

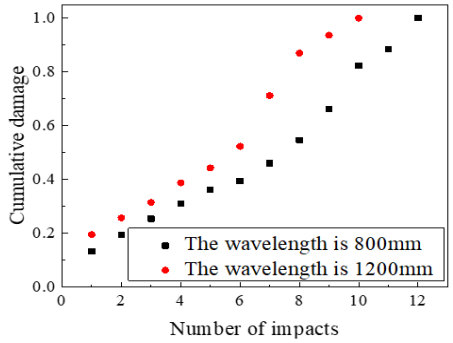

Fig. 7 Correlation between the quantity of impacts and total damage

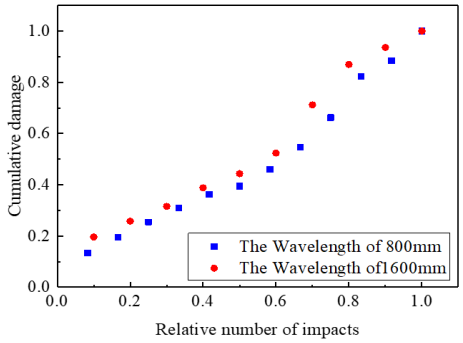

Fig. 8 Damage evolution pattern of C80 concrete specimens under repeated impacts

development - rapid rise."

(2) Analysis of damage to concrete specimens made of C80 at various impact velocities

Figs. 9-10 illustrates the relationship between the number of impacts and the cumulative damage caused by three impact velocities for repeated impacts of 800 mm and 1200 mm stress waves.

The aforementioned photos show the cumulative damage that the specimens underwent after receiving numerous impacts at 800 mm and 1200 mm stress wavelengths, respectively. Under the influence of repeated impacts at an 800 mm stress wavelength, the number of specimens' impact *resistance* decreased from 12 to 5, while the average impact velocity rose from 3.98 cm/s to 7.03 cm/s. The specimen was destroyed more quickly the faster the average impact velocity was. When the average impact velocity increased from 4.09 cm/s to 6.14 cm/s under the influence of repeated impact at 1200 mm stress wavelength, the impact resistance of the specimen decreased from 10 to 5, and the faster the damage to the specimen. Under the same stress wavelength, the number of the specimen's impact resistance is inversely proportional to the impact velocity; the higher the impact velocity, the lower the number of the specimen's impact resistance. The rate of

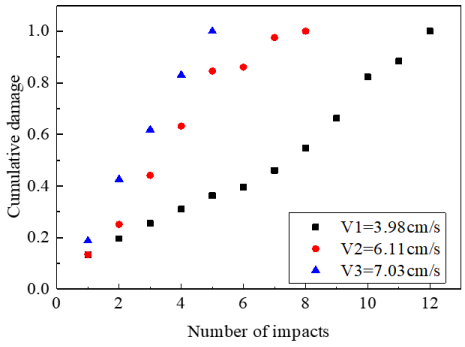

Fig. 9 800 mm stress wave

damage to the specimen is directly correlated with the impact velocity; the faster the impact velocity, the quicker the damage to the specimen.

3.4 C80 concrete damage evolution model

(1) Construction of the model

The Göpötz function curve exhibits a growth pattern characterized by "slowly developing - development of maturity - mature development", which is also the more

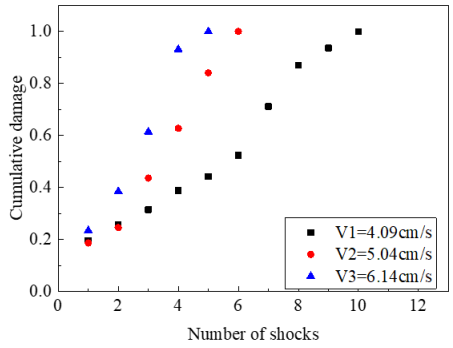

Fig. 10 1200 mm stress wave

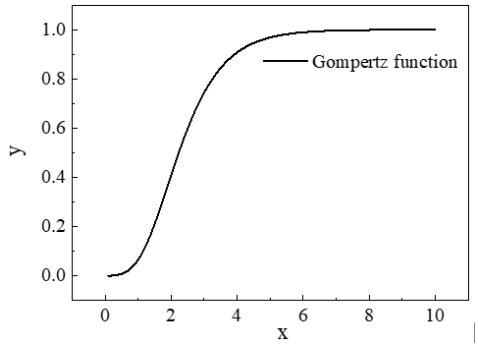

Fig. 11 Gompertz function curve

well-known S-shaped curve in the field of mathematics, are frequently stated in the social and economic sciences. The Goetz function curve has a shorter front end, a longer back end, and a logic function with features of intermediate symmetry. This is the major distinction between the two functions. The C80 concrete damage development trend is more in line with the characteristics of the Goetz function curve, having a shorter front portion and longer rear end. Fig. 11 depicts the Goetz function curve's shape.

The expression for the Goppertz function can be expressed as shown in Eq. (14).

$$y = A \cdot e^{-e^{-B(x-C)}} \tag{14}$$

A rough division into three stages can be made for the Goppertz function: slow development, fast development, and mature and smooth development. The three steps of the development law for C80 concrete under repeated impact are "rapid rise, smooth development, and rapid rise." By examining the similarities and differences between the two cases, it is possible to characterize the characteristics of the three stages of cumulative deterioration of C80 concrete using the inverse of the Goetz function. The inverse function of the Goetz function is shown in Eq. (15).

$$y = A - B \cdot ln\left(ln\frac{C}{x}\right) \tag{15}$$

Where: A, B, and C are parameters that need to be determined; x is an independent variable that shows how many times an impact occurs; and y is a dependent variable that shows how much damage has been done cumulatively. Therefore, Eq. (16) can be used to explain the damage development model applied to C80 concrete under repeated impacts in this research.

$$D = \delta - \alpha \cdot ln\left(ln\frac{\beta}{n}\right) \tag{16}$$

Eq. (16) can be given values, with α, β, and δ are taken as 0.15, 14, and 0.25, respectively, to get the graph in Fig. 12.

(2) Parameter determination

In Eq. (16), the damage variable (parameter D) has a value range of 0 to 1 and is used to investigate the physical relevance of the other three parameters. By maintaining two parameter values while changing another, the impact of parameter changes on the model curve is examined.

The impacts on the model curve when β and δ are fixed and α is taken to have values of 0.15, 0.25, 0.35, 0.45, and 0.55, the effects on the model curve are shown in Fig. 13. The smooth development section of the curve shortens as the value of α increases, gradually evolving from the obvious 3-stage characteristic to the exponential-like function type, Therefore, it can be seen that the effect of impact velocity on cumulative damage is reflected by the parameter α. The smaller the impact velocity, the smaller the α, In summary, it can be obtained that the physical meaning of the parameter α is the cumulative damage impact factor influenced by the impact velocity.

Fig. 14 depicts the effects on the model curve when α and δ are fixed and β values are taken as 14, 13, 12, 11, and 10, respectively. It can be inferred that the asymptote of the

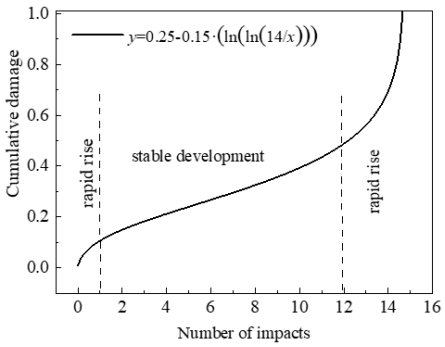

Fig. 12 C80 concrete repeated impact cumulative damage model curve

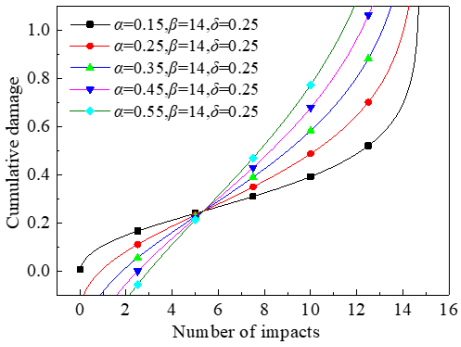

Fig. 13 Effect of variation of α on the model curve

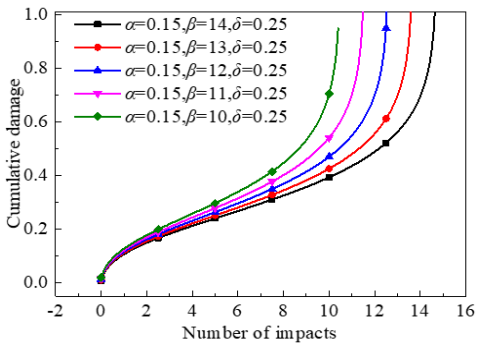

Fig. 14 Effect of variation of β on the model curve

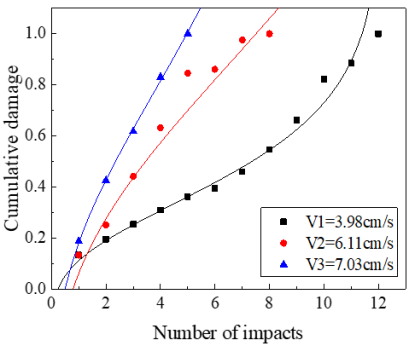

Fig. 16 800 mm stress wavelength

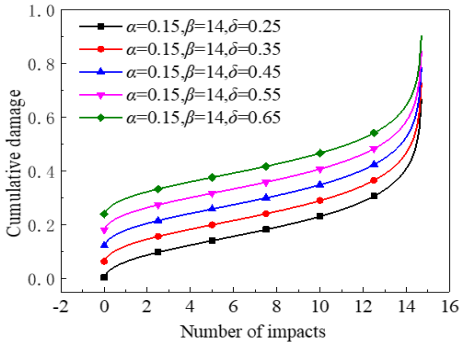

Fig. 15 Effect of variation of δ on the model curve

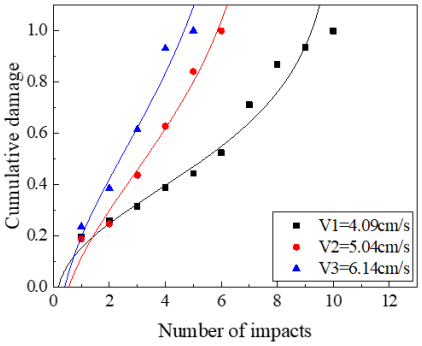

Fig. 17 1200 mm stress wavelength

end section of the curve is nearly equal to the value of β, and that β only affects the size of the endpoint of the independent variable in the later fast-growing section and has almost no impact on the earlier development, that is β controls the size of the value of the independent variable in the later fast-growing section. According to the test data, it can be obtained that the smaller the impact velocity, the most repeated impact number; with the gradual increase in impact velocity, the number of repeated impacts gradually decreases; In summary, the physical meaning of the β parameter is the cumulative damage impact factor affected by the number of impacts, when using the number of impacts as the independent variable, the value of β is the number of impacts under a particular condition.

When α and β are fixed and δ values are taken as 0.25, 0.35, 0.45, 0.55, and 0.65, respectively, the effect on the model curve is shown in Fig. 15. It can be obtained that the value of δ affects the initial development of cumulative damage, and the larger its value, the larger the value of damage in the initial stage. Therefore, the physical significance of the δ parameter is the cumulative damage model adjustment factor.

(3) Validating the model

Figs. 16-17 show how the model may depict the impacts of impact velocity and impact number on the total amount of damage. The damage evolution at an impact velocity of 3.98 cm/s under the action of an 800 mm stress wavelength has obvious three-stage characteristics, and the damage evolution at an impact velocity of 4.09 cm/s also has obvious three-stage characteristics. As the impact velocity increases, the development of cumulative damage gradually increases with the increase in velocity. When the impact velocity is 7.03 cm/s and 4.09 cm/s under the influence of two stress wavelengths, respectively, the cumulative damage changes with the rise in impact number most quickly, and the damage data points are the most sparse. The cumulative damage model developed in this study can adequately explain the law, and both the fit and correlation to the test data at each impact velocity are excellent.

According to the damage development model developed in this paper, Table 5 displays the values of the parameters suited to the cumulative damage of C80 concrete at various stress wavelengths and impact velocities

Table 5 shows that when the impact velocity increases and the number of impacts reduces, α and δ increase while the value of β drops. According to the physical significance of the parameters α and β, it means that with the increase of the impact velocity, the smooth development section of the accumulated damage gradually decreases, the initial stage

Table 5 Fitting parameter values at each stress wavelength

The stress wavelength (mm)	The impact velocity (cm/s)	α	β	δ	Correlation coefficient
800	V1	0.2425	12.15	0.3332	0.9913
	V2	0.6861	12.09	0.7503	0.9525
	V3	0.6926	10.08	0.761	0.9829
1600	V1	0.2684	10.18	0.3783	0.9771
	V2	0.4469	7.77	0.4355	0.9825
	V3	0.5151	7.03	0.5398	0.9669

damage development also increases with the increase of the impact velocity, and the number of repeated impacts decreases with the increase of the stress wavelength. The changes of parameters α, β and δ are consistent with their physical meanings.

4. Comparison of dynamic mechanical properties of C80 and C35 concrete

4.1 Dynamic mechanical parameters of C35 concrete

The C35 concrete specimen is Φ75×50 mm, and the end face's unevenness is within 0.02 mm. Table 6 displays the outcomes of the dynamic impact testing of SHPB using impact rod lengths of 40 0 mm, 600 mm, and 800 mm.

Fig. 18 illustrates the stress-strain correlations for C35 concrete corresponding to various impact bar lengths.

The characteristics depicted in Fig. 18 can be approximated by the curve shown in Fig. 19. Analysis of Fig. 19 indicates that the stress-strain behavior of C35 concrete under varying strain rates can be categorized into four distinct stages:

AB Stage (Elastic Stage): This stage is characterized by a linear increase in stress with strain, demonstrating elastic behavior. The initial dynamic elastic modulus is notably high, attributed to the brief duration of the stress pulse, which results in a rapid rise in stress without significant deformation.

BC Stage (Strain Softening Stage): With continued application of the stress pulse, internal deformation initiates, though the specimen remains intact. Stress increases at a slower rate while strain continues to accumulate, indicative of strain softening.

CD Stage (Elastic Recovery Stage): The stress-strain curve exhibits another linear ascent, akin to the AB stage, with a high dynamic elastic modulus. Internal pores within the concrete undergo deformation and closure under stress, leading to enhanced stiffness. The stress at point D corresponds to the yield stress. A higher yield stress under identical impact loading conditions suggests minimal internal damage and superior resistance to external impacts.

EF Stage (Post-Peak Failure Stage): A sharp decline in stress is observed as the specimen experiences internal damage under sustained external loading. This phase signifies the failure of the concrete.

4.2 Comparative analysis of stress-strain curves

Using the impact test with a 600 mm impact rod length as an example, the dynamic mechanical properties of C35 concrete and C80 high-strength concrete were investigated. Fig. 20 depicts the stress-strain correlations between the two materials at a strain rate of 50 s^{-1}.

Fig. 20 shows that under the influence of a dynamic load impact, the dynamic modulus of elasticity of C80 high-strength concrete is much larger than that of C35 concrete. For C80 high-strength concrete, the stress-strain relationship can be roughly split into three phases, while for C35 concrete, it can be roughly divided into five stages. The first peak value point of C80 high-strength concrete is significantly larger than that of C35 concrete in the first stage. After then, the stress-strain relationship between C80 high-strength concrete entered its second phase, which was characterized mostly by plastic deformation, with minimal

Table 6 Dynamic mechanical parameters of C35 concrete at each impact bar length

Number	Strength grade (MPa)	Impact bar length (mm)	Impact velocity (V/S)	Strain rate	Number	Strength grade (MPa)	Impact bar length (mm)
1	C35	400	3.70	32.06	23.83	3994.68	43.55
2			4.48	48.57	33.08	5474.20	190.95
3			5.07	20.64	44.64	6787.57	117.42
4			7.22	79.80	50.59	8928.29	101.20
5			8.07	87.06	61.86	9102.05	143.34
6			8.74	92.43	68.19	10666.42	198.62
7	C35	600	4.35	50.04	31.10	8439.58	65.14
8			5.38	54.56	41.78	9382.46	96.32
9			6.41	68.34	46.79	11289.58	97.21
10			7.07	75.47	58.15	11679.50	118.07
11			7.71	82.21	55.36	15044.79	192.60
12			8.36	81.82	67.23	15846.88	270.54
13	C35	800	3.52	34.04	34.82	6751.077	60.70
14			4.54	47.88	43.10	8815.614	82.73
15			5.57	60.86	61.63	8597.473	101.33
16			6.55	62.42	72.24	13781.91	115.83
17			7.15	69.79	75.13	16065.63	121.55

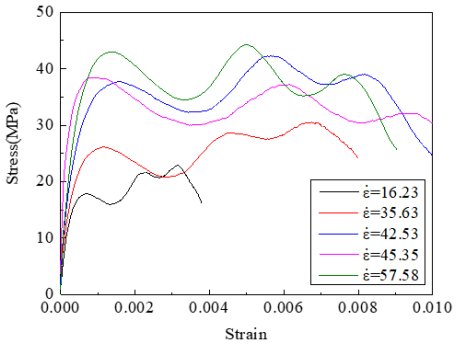

(a) Stress-strain curve for rod length of 400 mm

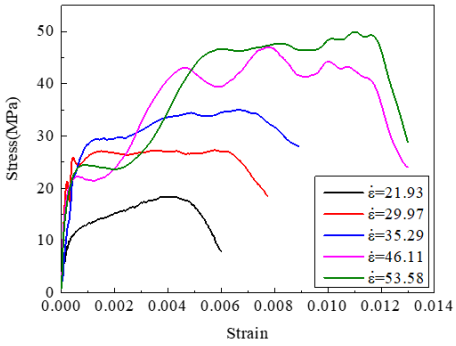

(b) Wind direction profile

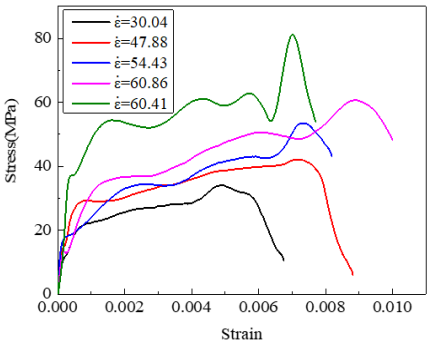

(c) Stress-strain curve for rod length of 800 mm

Fig. 18 Stress-strain curves under different impact rod

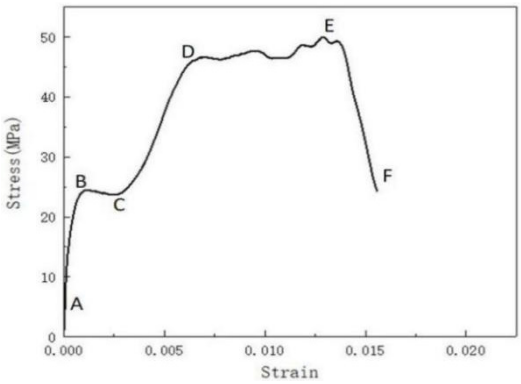

Fig. 19 Stress-strain curves of C35 concrete

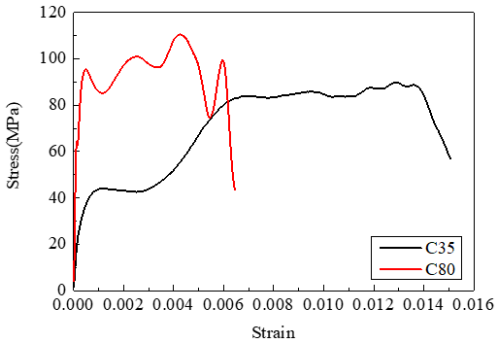

Fig. 20 Stress-strain curve of C35 and C80 concrete

overall growth in the performance of the stress and slow growth in the strain; The second phase of C35 concrete's stress-strain relationship underwent a prolonged development process, in which the stress essentially remained constant and the strain steadily grew. In the third phase, the C80 high-strength concrete reached the failure damage phase. And in the third stage, the stress strain of C35 concrete experienced another linear process of increasing development. The stress-strain of C35 concrete again has a flat development pattern in the fourth stage. The failure damage stage for C35 concrete is the fifth stage. Because C35 concrete has a lot of pores and will experience a closure process when subjected to external impact loading, while C80 high-strength concrete is relatively dense internally, no significant impact compression compacting process will occur in the third stage, explaining why C35 concrete experiences a linear increase in stress-strain development again while C80 high-strength concrete does not exhibit this phenomenon. Because coarse aggregate damage predominates in the damage stage of C80 high-strength concrete as opposed to the combination of coarse aggregate and cementitious material in C35 concrete, the stress-strain in the third stage of failure of C80 high-strength concrete tends to decrease linearly while the stress-strain in the fifth stage of failure of C35 concrete tends to decrease slowly.

4.3 Comparative analysis of strength characteristics

The peak stresses of the two materials may be determined for strain rates ranging from 50 s^{-1} to 80 s^{-1}, respectively, according to the dynamic impact tests of C35

Table 7 Peak stresses corresponding to different strain rates for C35 and C80 concrete

C35		C80	
Strain rate (s^{-1})	Peak stress (MPa)	Strain rate (s^{-1})	Peak stress (MPa)
44.22	19.92	46.11	47.43
50.04	31.10	50.68	55.75
53.92	39.62	51.92	56.62
54.56	41.78	52.67	64.35
60.41	43.04	53.97	65.46
60.59	41.02	57.01	57.85
63.04	46.24	58.67	65.38
68.34	46.79	59.66	71.95
68.83	37.87	60.69	73.03
70.40	49.87	61.37	62.05
72.61	48.82	63.29	70.50
75.47	58.15	64.95	67.68
76.34	45.28	66.06	75.51
81.83	52.08	67.48	64.29
82.22	55.37	68.10	73.12
/	/	70.82	65.78
/	/	71.41	70.75
/	/	80.35	84.52
/	/	81.83	77.61
/	/	85.46	90.14

concrete and C80 high-strength concrete, as shown in Table 7.

Additionally, as shown in Fig. 21, the peak stress-strain rate curves for C35 concrete and C80 high-strength concrete can be generated.

Fig. 21 shows that when the strain rate is the same under the influence of dynamic load impact, the peak stress of C80 high-strength concrete is generally equal to 1.5 times the peak stress of C35 concrete, demonstrating that C80 high-strength concrete has higher dynamic compressive strength. Since both types of concrete had a considerable strain rate effect, the peak stresses of the two-strength concrete specimens increased as the strain rate increased.

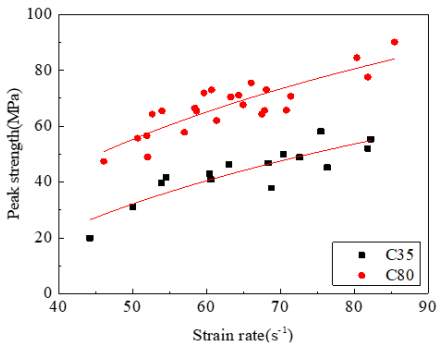

Fig. 21 Peak strength-strain rate curves for C35 and C80 concrete

Table 8 Dynamic modulus of elasticity of C35 and C80 concrete

C35		C80	
Strain rate (s^{-1})	Elasticity modulus (GPa)	Strain rate (s^{-1})	Elasticity modulus (GPa)
10.37	35.35	11.41	76.62
16.63	34.68	18.29	81.68
19.55	29.95	21.51	75.86
20.14	29.80	22.16	89.30
22.08	28.57	24.55	81.60
22.32	30.10	26.44	86.69
24.04	25.81	28.19	84.85
25.63	26.13	28.47	88.84
25.88	35.10	28.55	77.55
25.96	23.18	30.94	82.72
28.12	27.43	34.57	76.07
31.43	30.76	36.19	97.95
32.90	33.34	38.87	81.56
35.34	31.21	39.20	87.32
35.63	33.15	40.82	91.00
37.11	31.64	41.53	87.98
37.75	30.36	41.69	79.47
37.90	38.63	46.79	89.15
42.53	36.96	49.90	83.82
45.36	43.38	54.55	96.75
49.59	23.66	57.33	93.27
52.12	47.46	/	/
56.61	42.74	/	/
57.59	36.17	/	/

Indicating that the strengths of the two concrete materials grow similarly under the same strain rate increments is the fact that the slopes of the fitted peak stress-strain rate curves of the two strengths of concrete are essentially the same.

4.4 Comparative analysis of elastic modulus

The dynamic modulus of elasticity of C35 concrete and C80 high-strength concrete can be determined individually, as shown in Table 8, based on the dynamic impact tests.

The information in Table 8 was used to fit the dynamic modulus of elasticity-strain rate curves for various concrete strengths, as shown in Fig. 22.

Fig. 22 shows that the dynamic modulus of elasticity of the two concrete strength grades changes in a specific value range with an increase in strain rate under the influence of dynamic load impact, and the changing trend is not immediately apparent, indicating that the dynamic modulus of elasticity of the two concrete strength grades is not rated sensitive. The dynamic modulus of elasticity of concrete is closely related to the strength of concrete, as shown by the fact that the dynamic modulus of elasticity of C80 high-strength concrete is much greater than that of C35 concrete.

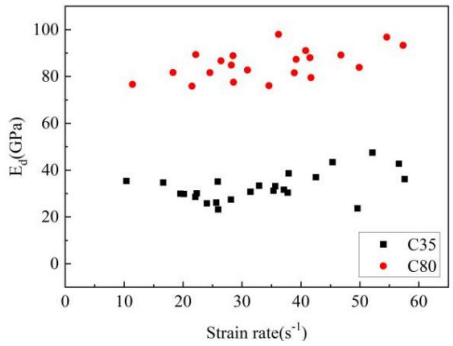

Fig. 22 Comparison of dynamic modulus of elasticity versus strain rate

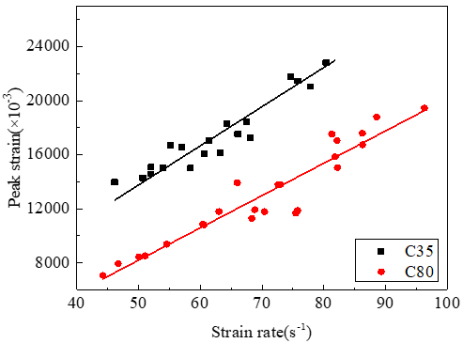

Fig. 23 Peak strain versus strain rate for C35 and C80 concrete

The cause of this is that typical concrete specimen have numerous internal pores, and when an external load is applied, these pores are forced outward, causing significant deformation and a low elastic modulus in the specimens. Although the elastic modulus of high-strength concrete is bigger, as the strength grows, the internal compactness of concrete increases, the number of aggregates also increases, the water-cement ratio is relatively reduced, and the internal pores are gradually reduced.

4.5 Comparative analysis of deformation characteristics

The average values of ultimate strains of C35 concrete and C80 high-strength concrete at strain rates of 50 s^{-1}, 60 s^{-1}, 70 s^{-1}, 75 s^{-1}, and 80 s^{-1} can be determined based on the dynamic impact tests of the two strength grades of concrete, as shown in Table 9.

Additionally, as shown in Fig. 23, the ultimate strain-strain rate curves for C35 concrete and C80 high-strength concrete can be generated.

Fig. 23 il lustrates how the ultimate stresses of concrete specimens of various strengths subjected to dynamic load impact all rise as the strain rate rises. The ultimate strain of C35 concrete is almost 1.5 times that of C80 high-strength concrete under the same strain rate, showing that the deformation of C35 concrete is more noticeable under this circumstance. Additionally, the slope of the ultimate strain strain rate curve for C35 concrete is substantially higher than it is for C80 high-strength concrete, indicating that high-strength concrete exhibits less rate sensitivity of deformation in addition to having a lower ultimate strain.

Table 9 Dynamic ultimate strains of C35 and C80 concrete under the action of similar strain rates

Strain rate (s^{-1})	Strain rate (s^{-1})	Ultimate strain ($\times10^{-6}$)
C35	50	1474
	60	1608
	70	1725
	75	2302
	80	2520
C80	50	8300
	60	1116
	70	1286
	75	1317
	80	1637

5. Conclusions

By systematically analyzing the dynamic mechanical properties of C80 concrete under the action of different stress wavelengths and different strain rates, the following conclusions can be obtained.

(1) Under the influence of different stress wavelengths and different impact speeds, the dynamic strength of C80 high-strength concrete is positively correlated with the strain rate, and the dynamic strength growth factor is positively correlated with the natural logarithm of the strain rate. The peak strain is also positively correlated with the strain rate, and the increase in stress wavelength and impact speed raises the overall trend of peak strain.

(2) When subjected to repeated impacts, C80 high-strength concrete exhibits a “rapid rise - smooth development - rapid rise” pattern in terms of cumulative damage and number of impacts. As impact speed increases, the cumulative damage increases significantly, while the number of repeated impacts gradually declines. The cumulative damage evolution model of C80 concrete can simultaneously express the impacts of impact velocity and impact number.

(3) Under the influence of a dynamic impact, the damage strength and ultimate strain of C80 high-strength concrete and C35 concrete both exhibit clear rate effect characteristics. The dynamic modulus of elasticity of both materials has no strain rate sensitivity but fluctuates up and down in a specific range. With an increase in strain rate, the dynamic modulus of elasticity of high-strength concrete is greater than that of ordinary concrete. For materials with substantially different strength grades, variations in water-to-binder ratio, aggregate-matrix interfacial properties, and microstructural characteristics may significantly alter the parameter sensitivity of the current model.

Data availability

The numerical data used to support the findings of this study are available from the corresponding author upon request.

Conflicts of interest

The authors declare that there are no conflicts of interest regarding the publication of this article.

Acknowledgments

This work was supported by the Henan Province science and technology research project (242102320010), and the Henan Province housing and urban and rural construction science and technology plan project(HNJS-2022-K3).

References

Antoniou, A., Daudeville, L. and Marin, P. (2025), "Extending the Discrete Element Method to Account for Dynamic Confinement and Strain-Rate Effects for Simulating Hard Impacts on Concrete Targets", *J. Dyn. Behavior Mater.*, **11**(1), 119-135. https://doi.org/ 10.1007/s40870-024-00438-6

Cao, Y.G., Zhao, G.X. and Yin, Y.Y. (2020), "Strength prediction of fiber reinforced polymer composite confined damaged concrete using general regression neural network", *Acta Materiae Compositae Sinica*, **24**(10), 1-6.

Caverzan, A., Peroni, M. and Solomos, G. (2016), "Compressive behaviour of dam concrete at higher strain rates", *Eur. Phys. J. Special Topics*, **225**(2), 283-293. https://doi.org/10.1140/epjst/e2016-02628-5

Chen, X., Wu, J., Shang, K., Ning, Y.J. and Bai, L.H. (2022), "Investigation of the Deformation and Failure Characteristics of High-Strength Concrete in Dynamic Splitting Tests", *Int. J. Concrete Struct. Mater.*, **16**(1), 1-18. https://doi.org/10.1186/s40069-022-00548-2

Du, Y., Qi, H.H., Jiang, J. and Richard, L.J. (2022), "Experimental study on the dynamic behaviour of expanded-shale lightweight concrete at high strain rate", *Mater. Struct.*, **55**(1), 1-17. https://doi.org/10.1617/s11527-021-01846-z

Huang, Z.P., Qiao, L., Zhou, M., Li, Q.W. and Yang, J.M. (2023), "Research on dynamic impact of concrete based on improved SHPB", *Eng. Blast.*, **29**(1), 19-68. https://doi.org/10.19931/j.EB.20210197

Kachanov, L.M. (1999), "Rupture time under creep conditions", *Int. J. Fract.*, **97**(1), 11-18.

Lata, P. (2021), "Stoneley wave propagation in an orthotropic thermoelastic media with fractional order theory", *Compos. Mater. Eng., Int. J.*, **3**(1), 57-70. https://doi.org/10.12989/cme.2021.3.1.057

Martin, B.E., Heard, W.F., Loeffler, C.M. and Nie, X. (2018), "Specimen size and strain rate effects on the compressive behavior of concrete", *Experim. Mech.*, **58**(2), 357-368. https://doi.org/10.1007/s11340-017-0355-2

Mohammad, M.K., Kamran and Mohd, A.I. (2024), "Compressive and tensile behaviour of concrete subjected to high rate of loading", *Innov. Infrastr. Solut.*, **9**(1), 1-22. https://doi.org/10.1007/s41062-023-01338-9

Parida, S.P. and Jena, P.C. (2023), "Selective layer-by-layer fillering and its effect on the dynamic response of laminated composite plates using higher-order theory", *J. Vib. Control*, **29**(11-12), 2473-2488. https://doi.org/10.1177%2F10775463221081180

Ping, Q., Ma, Q.Y. and Yuan, P. (2013), "Prediction for stress equilibrium time in rock SHPB test", *J. Vib. Shock*, **32**(12), 55-60. https://doi.org/10.11883/bzycj-2024-0152

Rabia, B., Daouadji, T.H. and Abderezak, R. (2021), "Effect of air bubbles in concrete on the mechanical behavior of RC beams strengthened in flexion by externally bonded FRP plates under uniformly distributed loading", *Compos. Mater. Eng., Int. J.*, **3**(1), 41-45. https://doi.org/10.12989/cme.2021.3.1.041

Rabotnov, Y.N. (1969), "Creep rupture", In: *Applied Mechanics: Proceedings of the Twelfth International Congress of Applied Mechanics*, Stanford University, August 26-31, 1968, pp. 342-349. https://doi.org/10.1007/978-3-642-85640-2_26

Samuel, N.M., Afonso, M.S. and Maria A.R. (2022), "Analytical and numerical study of failure in composite plates", *Compos. Mater. Eng., Int. J.*, **4**(1), 23-41. https://doi.org/10.12989/cme.2022.4.1.023

Sharma, N., Thakur, M.S., Upadhya, A. and Sihag, P. (2021), "Evaluating flexural strength of concrete with steel fibre by using machine learning techniques", *Compos. Mater. Eng., Int. J.*, **3**(3), 201-220. https://doi.org/10.12989/cme.2021.3.3.201

Tahwia, A.M., El-Far, O. and Amin, M. (2022), "Characteristics of sustainable high strength concrete incorporating eco-friendly materials", *Innov. Infrastr. Solut.*, **7**, 1-13. https://doi.org/10.1007/s41062-021-00609-7

Wang, D.R. and Hu, S.S. (2003), "Study on damage evolution of concrete under impact load", *Chinese J. Rock Mech. Eng.*, **22**(2), 223-226.

Zhang, L., Li, G.K. and Ma, W.H.F. (2020), "Fully implicit iterative method for the elastic-plastic damage problem of concrete-like materials", *J. Hydraulic Eng.*, **51**(8), 947-956.

Zhou, X., Wang, B.T. and Wu, Y.D. (2024), "Accuracy analysis of Young's modulus and stress-strain curve in the elastic stage of materials using Hopkinson bar experimental method", *Explos. Shock Waves*, **44**(9), 51-65. https://doi.org/10.11883/bzycj-2023-0380